

Small-Signal Modeling of Nonideal Magamp PWM Switch

Milan M. Jovanović, *Senior Member, IEEE*, and Laszlo Huber, *Member, IEEE*

Abstract—Circuit-based small-signal models of the magnetic amplifier (magamp) which include the effects of the nonideal squareness of the magamp's core B-H curve are derived for both the voltage-reset and current-reset control techniques. Since in this modeling approach the small-signal behavior of the magamp is described by equivalent circuits, circuit simulators can be easily used to facilitate the control-loop design optimization of the magamp.

Index Terms—B-H characteristic, control-loop interactions, magnetic amplifier, small-signal modeling.

I. INTRODUCTION

THE MAGNETIC amplifier (magamp) technique is one of the most reliable and cost-effective postregulation methods for multiple-output power supplies. This is especially true for high-current postregulated outputs since at higher output currents the efficiency of linear postregulators is unacceptably low, while the complexity of more efficient switch-mode postregulators is associated with a significant cost. Although in the past the magamps were used in numerous applications, their usage has dramatically increased with the introduction of 3.3-V integrated circuits (IC's). Namely, in today's data-processing equipment, which is based on both 3.3- and 5-V IC's (mixed-power designs), it is necessary to provide at least two high-current tightly regulated outputs. The most cost-effective approach to meet the tight-regulation requirements at both outputs is to directly regulate the 5-V output and postregulate the 3.3-V output using a magamp. Very often, in computer power supplies, the regulation requirements on the 12-V output, which is mainly used for driving the storage disk(s), warrant the use of a second magamp. As a result, today's multiple-output power supplies are complex control systems which contain multiple control loops that require suitable small-signal models for the control-loop performance optimization as well as for the analysis of possible loop interactions [1].

Various issues related to the operation, design, modeling, control, and simulations of magamps were discussed in [2]–[11]. However, while the operation of magamps with nonideal magamp-core materials was analyzed in [2] and [3], the small-signal analysis, modeling, and simulations of magamps have been, so far, exclusively carried out under

the assumption of the ideal squareness of the B-H curve of magamp's core material [4]–[11].

The objective of this paper is to introduce accurate circuit-based small-signal models of magamps which include the effects of the nonideal squareness of magnetic-core materials. Since, in this approach, the small-signal behavior of magamps is described by equivalent circuits, circuit simulators such as Spice and Saber can be easily used to facilitate the control-loop design optimization of magamps as well as perform their loop-interaction analysis.

II. KEY WAVEFORMS OF NONIDEAL MAGAMP

A simplified circuit diagram of a typical, two-output forward converter with a magamp postregulator is shown in Fig. 1. In this converter, the regulation of output voltage V_{o1} is achieved by a pulsewidth modulation (PWM) of the duty cycle of the primary switch S, whereas output voltage V_{o2} is regulated by a local magamp feedback loop, which modulates the duration of the blocking time of magamp inductor L_{MA} . It should be noted that the output of the magamp reset circuit $x_{Control}$ is control voltage v_C for the voltage-type reset, and reset current i_R for the current-type reset [3].

Fig. 2 shows the key waveforms of a nonideal magamp with the voltage reset, whereas Fig. 3 shows the assumed nonideal core B-H characteristics. The waveforms in Fig. 2 assume that load current $I_{o2} = \langle i_{LF2} \rangle$ is large compared to the magnetizing current of L_{MA} so that $i_{sec2} = i_{MA}$ is zero during the time intervals in which L_{MA} is not saturated and that L_{F2} is large so that the i_{LF2} ripple is negligible. It should be noted that the above assumptions greatly simplify the derivations of the models without compromising their accuracy.

As can be seen from Fig. 3, due to a nonideal squareness ($SQ = B_r/B_s < 1$) of the B-H curve, the magamp exhibits a small residual inductance when it is saturated. As a result, the commutation of output-filter inductor current i_{LF2} between forward diode D_{F2} and freewheeling diode D_{FW2} is not instantaneous as in the case of an ideal magamp ($SQ = 1$). Namely, as seen from Fig. 2, magamp current i_{MA} takes time to ramp up after L_{MA} becomes saturated at $t = t_1$, and also to ramp down after secondary voltage v_{sec2} becomes negative at $t = t_3$. In fact, during the commutation time $[t_3, t_4]$, during which i_{LF2} commutates from D_{F2} to D_{FW2} , the magamp core receives additional reset (additional volt seconds compared to ideal magamp) Λ_{sat} , as indicated in Fig. 2. This additional reset is caused by the commencement of the conduction of D_{FW2} at $t = t_3$ which clamps voltage v_A to zero during the entire commutation interval $[t_3, t_4]$.

Manuscript received November 5, 1997; revised March 1, 1999. Recommended by Associate Editor, O. Mandhana.

The authors are with the Power Electronics Laboratory, Delta Products Corporation, Research Triangle Park, NC 27709 USA.

Publisher Item Identifier S 0885-8993(99)07291-9.

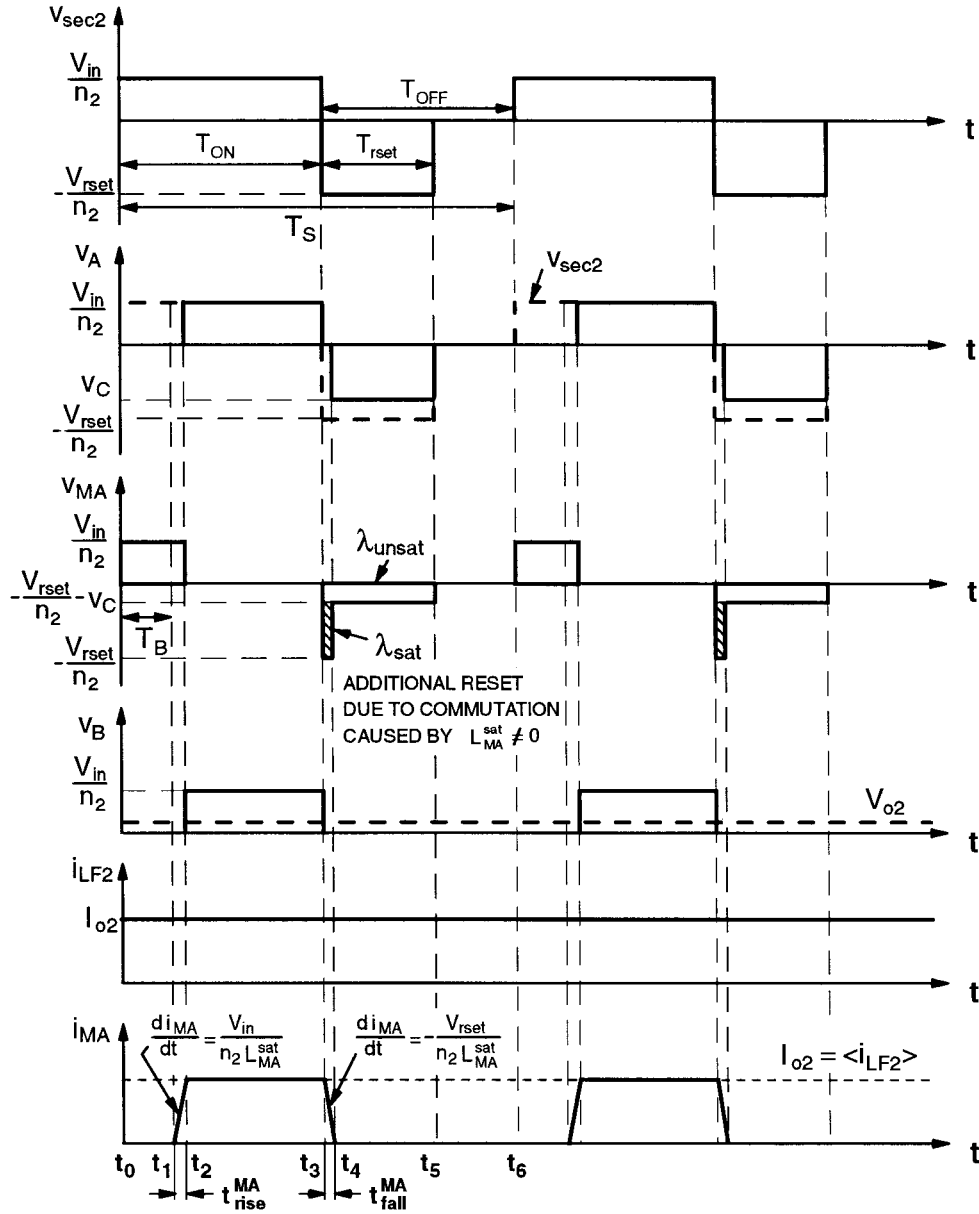


Fig. 2. Key waveforms of nonideal magamp with voltage reset ($x_{Control} = v_C$).

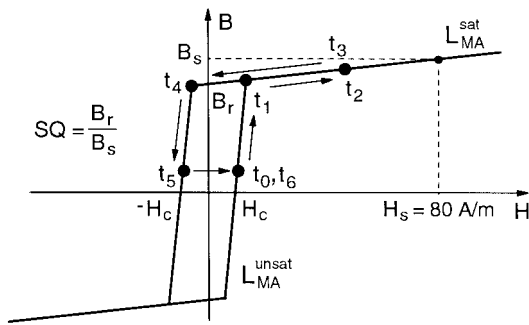


Fig. 3. Nonideal B-H characteristic. Squareness of characteristic defined as $SQ = B_r/B_s$, where B_s is measured at $H_s = 80$ A/m. Slopes of the B-H curve are proportional to unsaturated L_{MA}^{unsat} and saturated L_{MA}^{sat} inductances of the magamp.

should be noted that for the RCD-reset method of the forward-converter transformer core, reset voltage v_R is constant, i.e.,

it is independent of input voltage v_G . On the other hand, for the active-clamp reset technique, v_R is dependent on v_G . To simplify the analysis, in the following derivations, it is assumed that v_R is constant, i.e., $v_R = V_R$. As a result, the derived models represent approximate models for magamps operating in the forward converters with active-clamp reset.

Substituting (3) and (4) in (1) and (2), the average v_B and i_{MA} can be written as

$$v_B = v_G(d - d_B) - i_{LF}Z_S \tag{5}$$

$$i_{MA} = i_{LF}(d - d_B) - \frac{1}{2}i_{LF}^2Z_S \left[\frac{1}{v_G} - \frac{1}{V_R} \right]. \tag{6}$$

By perturbing the average quantities in (5) and (6) around their dc values (denoted with uppercase letters), i.e., by setting $v_G = V_G + \hat{v}_G$, $v_B = V_B + \hat{v}_B$, $d = D + \hat{d}$, $d_B = D_B + \hat{d}_B$, $i_{MA} = I_{MA} + \hat{i}_{MA}$, and $i_{LF} = I_{LF} + \hat{i}_{LF}$, where

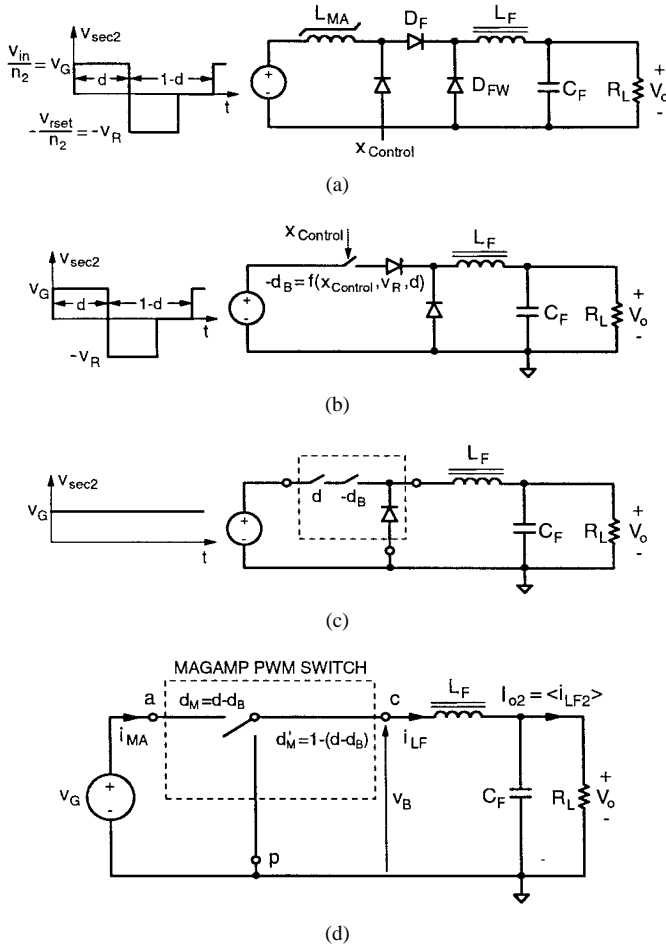


Fig. 4. Reduction of magamp to equivalent three-terminal PWM switch.

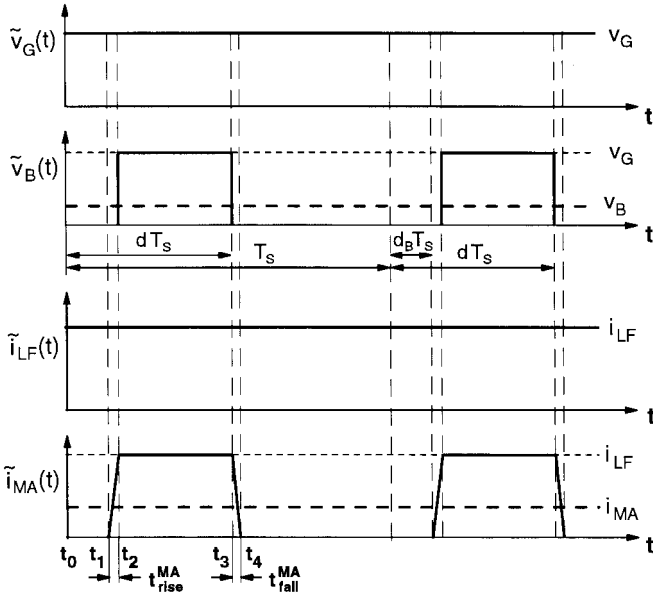


Fig. 5. Relationships between instantaneous and average terminal voltages and currents.

$\hat{\cdot}$ denotes a small-signal perturbation, the dc and small-signal models can be obtained.

From the perturbed (5) and (6), after a number of simple algebraic operations, the dc model of the magamp can be

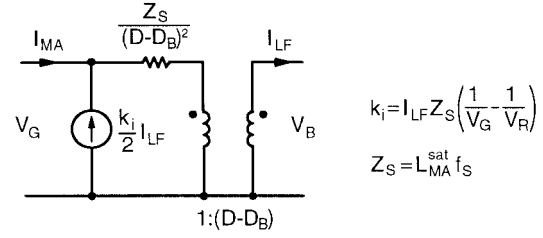


Fig. 6. DC equivalent-circuit model of magamp with nonideal core.

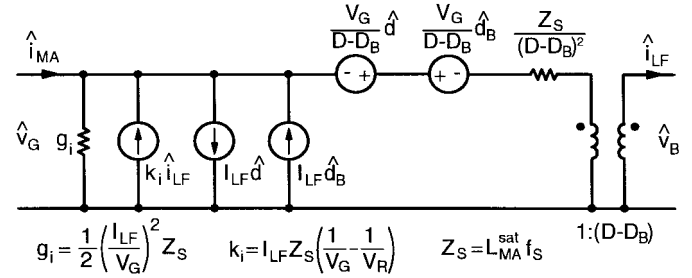


Fig. 7. Small-signal equivalent-circuit model of magamp with nonideal core.

extracted as

$$I_{MA} = I_{LF}(D - D_B) - \frac{1}{2} I_{LF}^2 Z_S \left[\frac{1}{V_G} - \frac{1}{V_R} \right] \quad (7)$$

$$V_B = V_G(D - D_B) - I_{LF} Z_S \quad (8)$$

whereas the small-signal model, after the second-order terms are neglected, is

$$\begin{aligned} \hat{i}_{MA} &= I_{LF}(\hat{d} - \hat{d}_B) + \hat{i}_{LF}(D - D_B) \\ &\quad - I_{LF} Z_S \left[\frac{1}{V_G} - \frac{1}{V_R} \right] \hat{i}_{LF} + \frac{1}{2} \left(\frac{I_{LF}}{V_G} \right)^2 Z_S \hat{v}_G \quad (9) \end{aligned}$$

$$\hat{v}_B = V_G(\hat{d} - \hat{d}_B) + \hat{v}_G(D - D_B) - Z_S \hat{i}_{LF}. \quad (10)$$

The set of equations describing the dc model can be represented by the equivalent circuit shown in Fig. 6, whereas the set of equations describing the small-signal model can be represented by the equivalent circuit shown in Fig. 7.

As can be seen from Fig. 6, the effect of the nonideal squareness of the core on the dc behavior of the magamp is modeled by the saturated inductance $Z_S/(D - D_B)^2$ and the current source $1/2 Z_S(1/V_G - 1/V_R) I_{LF}^2$. Since impedance Z_S is connected in series with the input and output terminals of the model, it makes the dc output voltage of the nonideal magamp dependent on the output current. Similarly, as can be seen from Fig. 7, the effect of the nonideal squareness of the core on the small-signal behavior of the magamp is modeled by impedance $Z_S/(D - D_B)^2$, current source $I_{LF} Z_S(1/V_G - 1/V_R) \hat{i}_{LF}$, and conductance $g_i = 1/2 (I_{LF}/V_G)^2 Z_S$. Due to Z_S and g_i , the small-signal transfer functions of the nonideal magamp are damped. This damping is not accounted for when ideal magamp core characteristics are assumed. It should be noted that the ideal dc and small-signal magamp models can be obtained from the models in Figs. 6 and 7 by setting $Z_S = 0$.

The small-signal equivalent circuit shown in Fig. 7 can be modified to include control variable $\hat{x}_{Control}$ instead of \hat{d}_B . To make this modification, it is necessary to find the functional

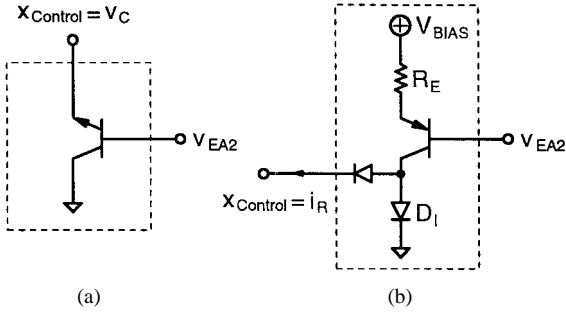


Fig. 8. Magamp reset circuit implementations: (a) voltage reset and (b) current reset.

relationship between control signal $x_{Control}$ and blocking duty cycle d_B . Generally, this functional relationship depends on the type of the magamp core reset circuit. The magamp reset circuit shown as a block in Fig. 1 can be implemented either by using the voltage reset of the magamp core, shown in Fig. 8(a), or the current reset, shown in Fig. 8(b). In the voltage-reset circuit, control voltage v_C , which is proportional to the error voltage v_{EA2} , is applied to the magamp core to obtain the desired core reset, i.e., to obtain the desired blocking time t_B . In the current-reset circuit, reset current i_R , which is proportional to the error voltage, is used to control the magamp reset.

B. Voltage Reset

From the v_{MA} waveform in Fig. 2, which represents the voltage across the magamp inductor with the voltage reset, the volt-second (flux) balance during the blocking and resetting time intervals yields

$$\frac{v_{in}}{n_2} T_B + \frac{v_{in}}{n_2} t_{rise}^{MA} = \left(\frac{v_{rset}}{n_2} + v_C \right) T_{rset} - v_C t_{fall}^{MA} \quad (11)$$

where T_{rset} is the reset time of the transformer core. This reset time can be calculated from the volt-second balance requirement of the transformer core, i.e., from

$$v_{in} T_{on} = v_{rset} T_{rset}. \quad (12)$$

After substituting t_{rise}^{MA} and t_{fall}^{MA} from (3) and (4) and T_{rset} from (12) in (11), the relationship between \hat{d}_B and \hat{v}_C can be derived as

$$\hat{d}_B = \left(1 + \frac{V_C}{V_R} \right) \hat{d} + \left(1 + \frac{V_C}{V_R} \right) \frac{Z_S I_{LF}}{V_G^2} \hat{v}_G - \left(1 + \frac{V_C}{V_R} \right) \frac{Z_S \hat{i}_{LF}}{V_G} + \frac{D_B}{V_C + V_R} \hat{v}_C. \quad (13)$$

Using the relationship given in (13) to eliminate \hat{d}_B in the equivalent circuit in Fig. 7, the equivalent circuit, small-signal model of the magamp with voltage reset shown in Fig. 9 is obtained. Since all the dependent current and voltage sources in this model are controlled by currents or voltages, the implementation of this model in circuit simulators is easier compared to the model in Fig. 7, whose implementation requires additional modeling steps.

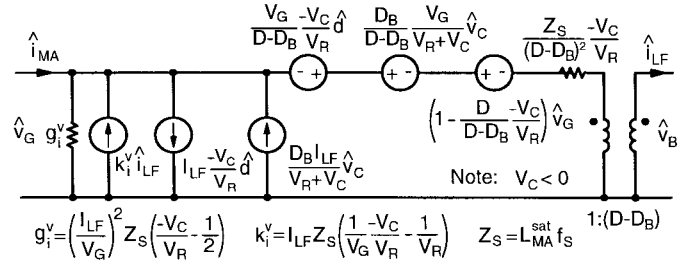


Fig. 9. Equivalent small-signal circuit of nonideal magamp with voltage reset.

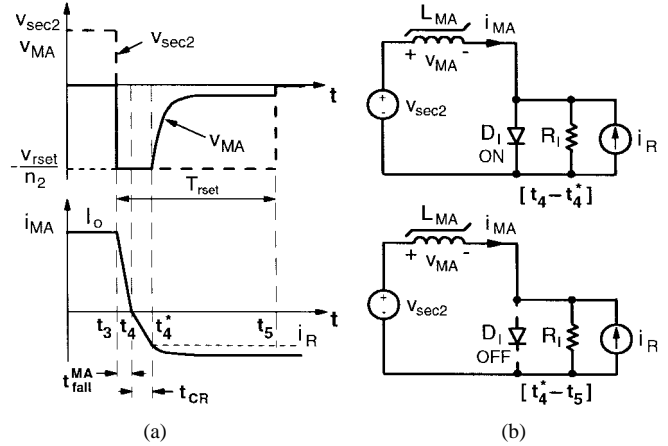


Fig. 10. Magamp with current reset: (a) v_{sec2} , v_{MA} , and i_{MA} waveforms and (b) topological stages during reset time. Note that reset current (negative i_{MA}) is much smaller than the load current so that it can be neglected. In this figure, it is shown much larger for clarity.

C. Current Reset

The major difference between the current reset and voltage reset of the magamp is seen in the magamp voltage waveform v_{MA} during the magamp reset interval. Fig. 10 shows the v_{sec2} , v_{MA} , and i_{MA} waveforms of a magamp with the current reset, along with the equivalent circuits of the magamp during different phases of the reset. The other waveforms of the magamp with the current reset are identical with those for the voltage reset shown in Fig. 2. It should be noted that in Fig. 10(b) the current reset circuit shown in Fig. 8(b) is modeled by an ideal current source i_R with output resistance R_I in parallel.

As can be seen from Fig. 10(a), the reset period can be divided into three intervals. During the $[t_3 - t_4]$ interval, i_{MA} linearly decreases from I_o toward zero and $v_{MA} = -v_{rset}/n_2$. In this interval, the behavior of the magamp with current reset is identical to that of the voltage reset. After i_{MA} reaches zero at $t = t_4$, diode D_I in the reset circuit in Fig. 8(b), continues to conduct i_R because the current through unsaturated L_{MA} can not increase (in the negative direction) instantaneously. Because of the diode conduction, $v_{MA} = -v_{rset}/n_2$, as shown in Fig. 10. When i_{MA} reaches i_R at $t = t_4^*$, diode D_I ceases conducting, and voltage v_{MA} starts exponentially decreasing with time constant $\tau = L_{MA}^{\text{unsat}}/R_I$, as shown in Fig. 10(a). At $t = t_5$, the transformer reset is finished so that $v_{MA} = 0$. It should be noted that the current reset requires that unsaturated inductance L_{MA}^{unsat} of magamp be finite, i.e., that the slope of

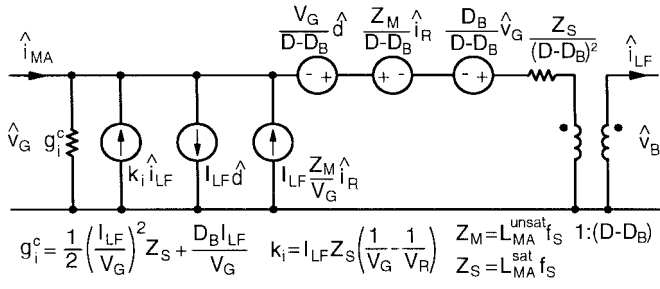


Fig. 11. Equivalent small-signal circuit of nonideal magamp with current reset.

B-H curve in the unsaturated region be less than ∞ (nonideal core).

Assuming that $\tau \ll T_{\text{rset}}$, i.e., assuming that the reset circuit in Fig. 8(b) approaches an ideal current source, the approximation of the volt-second balance on L_{MA} can be obtained from the v_{MA} waveform in Figs. 2 and 10(a) as

$$\frac{v_{in}}{n_2} T_B + \frac{v_{in}}{n_2} t_{\text{rise}}^{MA} = \frac{V_{\text{rset}}}{n_2} t_{\text{fall}}^{MA} + \frac{V_{\text{rset}}}{n_2} t_{CR} \quad (14)$$

where t_{CR} is calculated from Fig. 10(b) when diode D_I is conducting as

$$t_{CR} = \frac{L_{MA}^{\text{unsat}} i_R}{V_{\text{rset}}/n_2} = \frac{L_{MA}^{\text{unsat}} i_R}{V_R}. \quad (15)$$

Substituting t_{rise}^{MA} and t_{fall}^{MA} from (3) and (4), and t_{CR} from (15) into (16), the small-signal relationship between \hat{d}_B and \hat{i}_R can be derived as

$$\hat{d}_B = \frac{Z_M}{V_G} \hat{i}_R - \frac{D_B}{V_G} \hat{v}_G. \quad (16)$$

Using the relationship in (16) to eliminate \hat{d}_B in equivalent circuit in Fig. 7, the equivalent circuit, small-signal model of the magamp with current reset shown in Fig. 11 is obtained.

It should be noted that the presented models do not take into account the phase shift of the magamp modulator [4]. As a result, they are only accurate at frequencies at which the modulator phase shift can be neglected. Since for practical magamp implementations the modulator phase shift becomes important at frequencies above the crossover frequencies of the magamp loop, the derived models are quite accurate in predicting the close loop behavior of practical magamps. If necessary, the modulator phase shift as well as the B-H curve dynamic resistance [4], [5] can be incorporated into the models.

Finally, it should be noted that the modulator gain of the primary switch and its circuit implementations are discussed in [13] and [14].

IV. MODEL VERIFICATION

The experimental verifications of the derived models were performed on an off-line 100-W two-output power supply implemented with a 100-kHz forward-converter power stage. The main output, implemented with the current-mode control, is rated at $V_{o1} = 5$ V and $I_{o1} = 16$ A, whereas the rating of the magamp-regulated output is $V_{o2} = 3.3$ V and $I_{o2} = 6$ A.

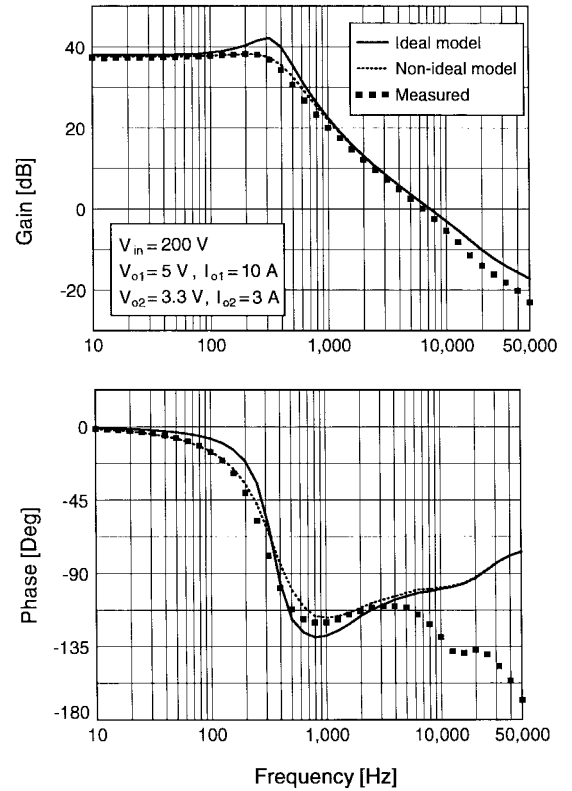


Fig. 12. Measured and simulated small-signal control-to-output transfer functions ($\hat{v}_{o2}/\hat{i}_R @ \hat{v}_G = 0$) for experimental magamp with current reset. Main-loop crossover frequency $f_C = 8.5$ kHz and magamp-loop crossover frequency $f_C^{MA} = 2.5$ kHz.

The magamp inductor was implemented with the MS $12 \times 8 \times 4.5$ -W Toshiba core with six turns of AWG#18 magnet wire. The current-reset method is used to reset the magamp core.

Fig. 12 shows the measured and simulated (ideal and nonideal) control-to-output characteristics of the experimental magamp with current reset. The values of the relevant circuit parameters and the parameters of the nonideal and ideal models are given in Tables I and II. The saturated and unsaturated inductances of the magamp, L_{MA}^{sat} and L_{MA}^{unsat} , were estimated from the measured B-H characteristic at 100 kHz. As it can be seen from Fig. 12, the measured amplitude and phase characteristics are in good agreement with the corresponding simulated characteristics obtained using the proposed nonideal magamp small-signal model. The proposed nonideal model accurately models the damping in the control-to-output transfer function. The discrepancy between the measured phase and the predicted phase which is observed at frequencies above 5 kHz is caused by the phase shift of the modulator, which is not included in the model given in Fig. 11. Because the crossover frequency of the main loop of 8.5 kHz is higher than that of the magamp loop which is approximately 2.5 kHz, no measurable interaction between the loops is noticeable in Fig. 12.

If the crossover frequency of the main loop is reduced below the crossover frequency of the magamp loop, the two loops exhibit strong interactions. Fig. 13 shows the simulated and measured control-to-output transfer functions of the experimental converter when the crossover frequency of the main loop is reduced to 0.1 kHz, i.e., below the crossover

TABLE I
CIRCUIT PARAMETERS OF EXPERIMENTAL CONVERTER

L_{F1} [μH]	ESR_{LF1} [$\text{m}\Omega$]	C_{F1} [μF]	ESR_{CF1} [$\text{m}\Omega$]	L_{F2} [μH]	ESR_{LF2} [$\text{m}\Omega$]	C_{F2} [μF]	ESR_{LF2} [$\text{m}\Omega$]	f_s [kHz]
11	10	1900	85	44	14	4700	28	100
N_P	N_{S1}	N_{S2}	V_G [V]	V_R [V]	D	D_B	L_{MA}^{sat} [μH]	L_{MA}^{unsat} [mH]
32	3	3	18.75	21	0.295	0.09	0.54	0.8

TABLE II
SMALL-SIGNAL MODEL PARAMETERS OF EXPERIMENTAL CONVERTER

MODEL	g_i^c [mS]	k_i	I_{LF} [A]	$I_{LF} \frac{Z_M}{V_G}$	$\frac{V_G}{D-D_B}$ [V]	$\frac{Z_M}{D-D_B}$ [Ω]	$\frac{D_B}{D-D_B}$	$\frac{Z_S}{(D-D_B)^2}$ [Ω]
NON-IDEAL	15.1	$9.26 \cdot 10^{-4}$	3	12.8	91.5	390	0.44	1.285
IDEAL	14.4	0	3	12.8	91.5	390	0.44	0

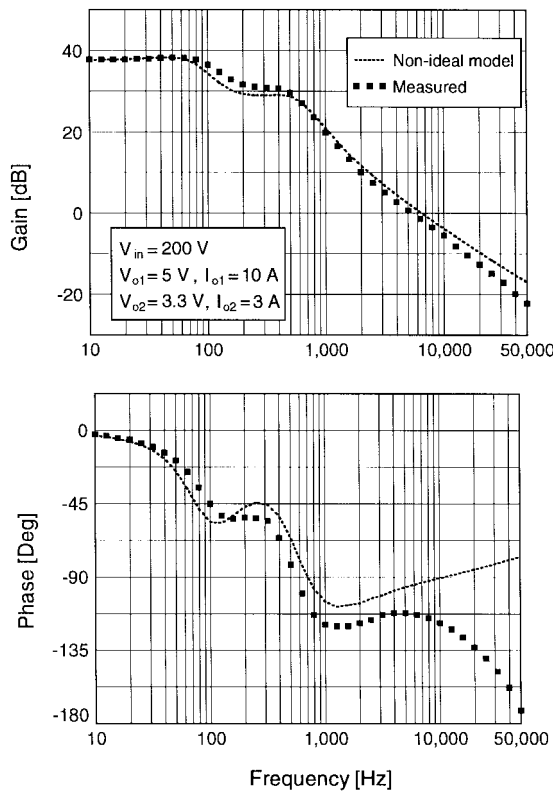


Fig. 13. Measured and simulated small-signal control-to-output transfer functions ($\hat{v}_{o2}/\hat{i}_R @ \hat{v}_G = 0$) for experimental magamp with current reset. Main-loop crossover frequency $f_C = 0.1$ kHz and magamp-loop crossover frequency $f_C^{MA} = 2.5$ kHz.

frequency of the magamp loop. As can be seen from Fig. 13, the main loop affects the control-to-output transfer function of the magamp by reducing its gain in the 80–500-Hz range. The agreement between the simulated and measured gain is very good up to 10 kHz, whereas the simulated and measured phase

show good agreement up to approximately 6 kHz. Above 6 kHz, the modulator phase lag becomes significant.

It should be noticed that besides the saturated impedance (Z_S) of the magamp, the load resistance, the resistances of the output filter, and the parasitic interconnect resistances on the secondary side, the winding loss and the core loss of the magamp also contribute to the damping in the control-to-output transfer function. The winding loss of the magamp can be easily included in the model by adding the winding resistance in series with the saturation impedance of the magamp. In the experimental circuit, the ac resistance of the magamp winding was approximately 3 m Ω and it was neglected compared to $Z_S = 54$ m Ω . The core loss, which is usually dominated by the winding loss at larger load current, has not been taken into account in the developed model. However, if necessary, the core loss can be incorporated into the model as proposed in [5]. It should be also noticed that the parasitic inductances in series with the magamp such as the leakage inductance of the transformer and layout inductances have the same effect on the small-signal model of the magamp as saturated inductance of the magamp L_{MA}^{sat} . Since in the experimental circuit these parasitic inductances were much smaller than the saturated inductance of the magamp, they were neglected. If necessary, the effect of the leakage inductance of the transformer and interconnect inductance can be easily taken into account by increasing the value of saturated magamp inductance L_{MA}^{sat} for the amount of the parasitic inductances.

V. SUMMARY

Circuit-based small-signal models of magamps which are suitable for the analysis of control-loop interactions in multiple-output power supplies are derived. The models include the effects of the nonideal squareness of the magnetic-switch-core B-H curve and also account for the differences in small-signal characteristics of the voltage-reset and current-

reset techniques. Since the small-signal behavior of magamps is described by equivalent circuits, circuit simulators can be easily used to facilitate the control-loop design optimization of the magamp.

REFERENCES

- [1] C. Jamerson and A. Hosseini, "Techniques for reduction of control-loop interactions in magamp supplies," Magnetics, Inc., Application Note, 1995.
- [2] C. Mullett and R. Hiramatsu, "An improved parallel control circuit for saturable reactor output regulators in high-frequency switch-mode converters," in *IEEE Applied Power Electronics Conf. (APEC) Proc.*, 1986, pp. 99–106.
- [3] R. M. Tedder, "Effects of converter type, reset method, and core material on magamp regulator performance," in *IEEE Applied Power Electronics Conf. (APEC) Proc.*, 1989, pp. 391–400.
- [4] R. D. Middlebrook, "Describing function properties of a magnetic pulse-width modulator," in *IEEE Power Electronics Specialists' Conf. (PESC) Rec.*, 1972.
- [5] T. Nabeshima, K. Harada, R. Hiramatsu, T. Kohchi, and S. Komatsu, "On the control of magnetic amplifier for high-frequency dc-to-dc converter," in *IEEE Int. Telecommunications Energy Conf. (INTELEC) Proc.*, 1985, pp. 449–454.
- [6] A. M. Urling, T. G. Wilson, H. A. Owen, G. W. Cromwell, and J. Paulakonis, "Modeling the frequency-domain behavior of magnetic-amplifier-controlled high-frequency switched-mode power supplies," in *IEEE Applied Power Electronics Conf. (APEC) Proc.*, 1987, pp. 19–31.
- [7] C. Jamerson, "Calculation of magnetic amplifier post regulator voltage control loop parameters," in *High-Frequency Power Conversion (HFPC) Conf. Proc.*, 1987, pp. 222–234.
- [8] D. Y. Chen, J. Lee, and C. Jamerson, "A simple model predicts small-signal control loop behavior of magamp post regulator," in *High-Frequency Power Conversion (HFPC) Conf. Proc.*, 1988, pp. 69–84.
- [9] I. J. Lee, D. Y. Chen, Y. P. Wu, and C. Jamerson, "Modeling of control loop behavior of magamp post regulators," in *IEEE Int. Telecommunications Energy Conf. (INTELEC) Proc.*, 1989.
- [10] V. J. Thottuvelil, "Using SPICE to model the dynamic behavior of dc-to-dc converters employing magnetic amplifiers," in *IEEE Applied Power Electronics Conf. (APEC) Proc.*, 1990, pp. 750–759.
- [11] D. Edry and S. Ben-Yaakov, "A SPICE model of magamp post regulators," in *IEEE Applied Power Electronics Conf. (APEC) Proc.*, 1992, pp. 793–800.
- [12] V. Vorperian, "Simplified analysis of PWM converters using the model of the PWM switch: Part I and II," *IEEE Trans. Aerosp. Electron. Syst.*, vol. 26, no. 3, pp. 490–505, 1990.
- [13] R. B. Ridley, "A new, continuous-time model for current-mode control," *IEEE Trans. Power Electron.*, vol. 6, pp. 271–280, Apr. 1991.
- [14] V. Vorperian, "Analysis of current-mode controlled PWM converters using the model of the current-controlled PWM switch," in *Power Conversion & Intelligent Motion Conf. (PCIM)*, 1990, pp. 183–195.



Milan M. Jovanović (S'86–M'89–SM'89) was born in Belgrade, Yugoslavia. He received the Dipl. Ing. degree in electrical engineering from the University of Belgrade, Belgrade.

Presently, he is the Vice President for Research and Development of Delta Products Corporation, Research Triangle Park, NC, the U.S. subsidiary of Delta Electronics, Inc., Taiwan, R.O.C., one of the world's largest manufacturers of power supplies. His current research is focused on power conversion and management issues for portable data-processing equipment, design optimization methods for low-voltage power supplies, distributed power systems, and power-factor-correction techniques.



Laszlo Huber (M'86) was born in Novi Sad, Yugoslavia, in 1953. He received the Dipl. Eng. degree from the University of Novi Sad, Novi Sad, the M.S. degree from the University of Niš, Niš, Yugoslavia, and the Ph.D. degree from the University of Novi Sad in 1977, 1983, and 1992, respectively, all in electrical engineering.

From 1977 to 1992, he was an Instructor at the Institute for Power and Electronics, University of Novi Sad. In 1992, he joined the Virginia Power Electronics Center at Virginia Tech, Blacksburg, as a Visiting Professor. From 1993 to 1994, he was a Research Scientist at the Virginia Power Electronics Center. Since 1994, he has been a Senior Design Engineer at the Power Electronics Laboratory, Delta Products Corporation, Research Triangle Park, NC, the Advanced R&D unit of Delta Electronics, Inc., Taiwan, R.O.C., one of the world's largest manufacturers of power supplies. His 22-year experience includes the analysis and design of high-frequency high-power-density single-phase and three-phase power processors; modeling, evaluation, and application of high-power semiconductor devices; and modeling, analysis, and design of analog and digital electronics circuits. He has published more than 60 technical papers, holds one U.S. patent, and has two U.S. patents pending.